Differential Cross Sections for Positronium Formation in Positron - Hydrogen Scattering

By:

Mohd. Zahurin Mohamed Kamali
and
Kuru Ratnavelu

(Paper presented at the ***XIV International Workshop on Low Energy Positron and Positronium Physics & XV International Symposium on Electron-Molecule Collisions and Swarms*** held on 2-4 August 2007 at the University of Reading, United Kingdom, England)

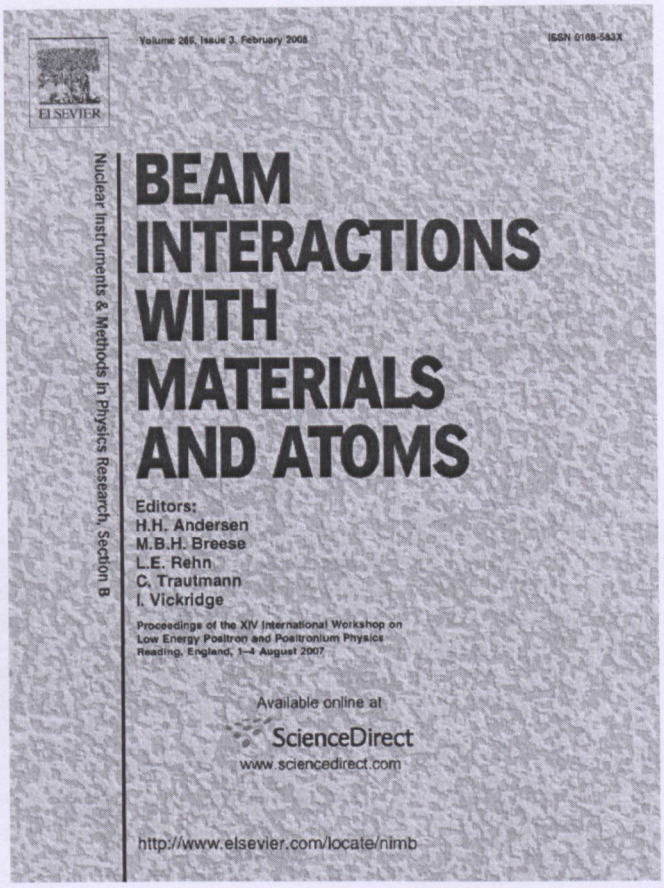

Available online at www.sciencedirect.com
ScienceDirect
Nuclear Instruments and Methods in Physics Research B 266 (2008) 388–392
NIM B
Beam Interactions with Materials & Atoms
www.elsevier.com/locate/nimb

Differential cross sections for positronium formation in positron–hydrogen scattering

M.Z.M. Kamali [a,*], Kuru Ratnavelu [b]

[a] Centre for Foundation Studies in Science, University of Malaya, 50603 Kuala Lumpur, Malaysia
[b] Institute of Mathematical Sciences, University of Malaya, 50603 Kuala Lumpur, Malaysia

Available online 15 December 2007

Abstract

Positron scattering by hydrogen atom is an interesting system to test theoretical methods due to its simplicity. Recently, theoretical calculations have reported differential cross sections (DCS) for positronium (Ps) formation for this system. The present work utilises the coupled-channel optical method (CCOM) that allows simultaneous treatment of the target channels and the Ps channels in the close-coupling method and the incorporation of the continuum effects via an optical potential to provide a comparative view of the DCS for Ps(1s) formation and Ps(2s) formation at energies ranging from 20 to 100 eV. A large 12-states and 15-states CCOM calculations have been undertaken and the results compared with other available data.

PACS: 34.85.+x; 34.10.+x

Keywords: Positronium (Ps) formation; Differential cross section; Positron scattering

1. Introduction

With the advent of major experimental breakthroughs in the last two decades [1,2], there has been growing theoretical and experimental interest in the positron scattering by atomic hydrogen [3–5]. In tandem, there has been a lot of progress in the theoretical studies of positron–hydrogen atomic system. One of the main reasons is the development of efficient computational techniques that has made it practical to do theoretical investigations with much ease [3,4,6].

Even though it is the simplest three-body Coulomb system, the difficulties inherent in studying scattering of positrons with hydrogen atoms are quite well known. The interactions governing the positron and electron scattering processes leads to different dynamic mechanisms: such as the Ps formation that characterizes the uniqueness of the positron-scattering problem.

With the judicious use of suitable array of pseudostates [3,4], various calculations have been performed to accurately profile quantitatively and qualitatively the observables for the e^+–H scattering system. These calculations of Mitroy (CC($\overline{28}$,3)) [3] and Kernoghan et al. (CC($\overline{30}$,3)) [4] are considered as the benchmark calculations for e^+–H with high quality data for the elastic, inelastic and Ps formation processes.

Since the late 1990s, there have been attempts to use the optical potential method to study this system. Among them is the CCOM used by Ratnavelu et al. [7–9] within the close-coupling (CC) formalism [10] to study the e^+–H scattering. The CCOM provides a novel approach [11] to include the neglect of higher discrete and continuum channels in the CC calculation. There have been other theoretical methods such as the distorted wave methods of Mandal et al. [12–14] which have investigated the Ps formation (Ps(1s), Ps(2s), Ps(2p)) DCS in the e^+–H case. As a perturbative method, the distorted wave method has the capability in predicting reliable results at intermediate and higher energies. In view of the recent calculations

* Corresponding author. Tel.: +60 3 79675945; fax: +60 3 79576478.
E-mail address: mzmk2000@yahoo.com (M.Z.M. Kamali).

0168-583X/$ - see front matter © 2007 Elsevier B.V. All rights reserved.
doi:10.1016/j.nimb.2007.12.015

[12] for Ps formation DCS, the present CCOM calculations have been attempted to provide a comparative set of DCS at various intermediate and high energies. Due to the experimental challenges in measuring DCS for this system, there has been a glaring lack of reports on the DCS.

2. Theory

The theoretical details of the CCOM for positron-scattering by atomic hydrogen had been detailed elsewhere [7,9]. However, for completeness, a brief outline of the CCOM is presented here.

In e^+–H scattering collision process, the following reactions are possible, such as elastic scattering, inelastic scattering, Ps formation and ionization. The total wave function of the e^+–H system, as expanded in an eigenfunction expansion of the positron-scattering states $F_\alpha(\mathbf{r}_2)$ and the Ps states $\phi_\beta(\rho)$ which are coupled to the atomic states $\psi_\alpha(\mathbf{r}_1)$, is written as

$$\Psi(\mathbf{r}_1,\mathbf{r}_2) = \sum_\alpha \psi_\alpha(\mathbf{r}_1)F_\alpha(\mathbf{r}_2) + \sum_\beta \phi_\beta(\boldsymbol{\rho})G_\beta(\mathbf{R}), \tag{1}$$

where $\mathbf{r}_1$ and $\mathbf{r}_2$ represents the coordinates of e^- and e^+ with respect to the proton respectively. The relative ($\boldsymbol{\rho}$) and center of mass ($\mathbf{R}$) coordinates are defined as

$$\boldsymbol{\rho} = \mathbf{r}_1 - \mathbf{r}_2; \quad \mathbf{r}_1 = \mathbf{R} + \frac{\boldsymbol{\rho}}{2}; \quad \mathbf{R} = \frac{\mathbf{r}_1 + \mathbf{r}_2}{2};$$
$$\mathbf{r}_{12} = |\mathbf{r}_1 - \mathbf{r}_2|; \quad \mathbf{r}_2 = \mathbf{R} - \frac{\boldsymbol{\rho}}{2}. \tag{2}$$

Following standard procedures [9–11], the Schrodinger equation can be transformed into a coupled set of momentum space Lippmann–Schwinger (LS) equations for a positron with the momentum $\mathbf{k}$ incident on a hydrogen atom in state ψ_α:

$$\langle \mathbf{k}'\psi_{\alpha'}|T|\mathbf{k}\psi_\alpha\rangle = \langle \mathbf{k}'\psi_{\alpha'}|V^{(Q)}|\mathbf{k}\psi_\alpha\rangle + \sum_{\alpha'}\int \mathrm{d}^3k'' \frac{\langle \mathbf{k}'\psi_{\alpha'}|V^{(Q)}|\mathbf{k}''\psi_{\alpha'}\rangle\langle \mathbf{k}''\psi_{\alpha'}|T|\mathbf{k}\psi_\alpha\rangle}{\left(E^{(+)} - \epsilon_{\alpha''} - \frac{1}{2}k''^2\right)} + \sum_{\beta''}\int \mathrm{d}^3k'' \frac{\langle \mathbf{k}'\psi_{\alpha'}|V|\mathbf{k}''\phi_{\beta''}\rangle\langle \mathbf{k}''\phi_{\beta''}|T|\mathbf{k}\psi_\alpha\rangle}{\left(E^{(+)} - \epsilon_{\beta''} - \frac{1}{4}k''^2\right)}, \tag{3}$$

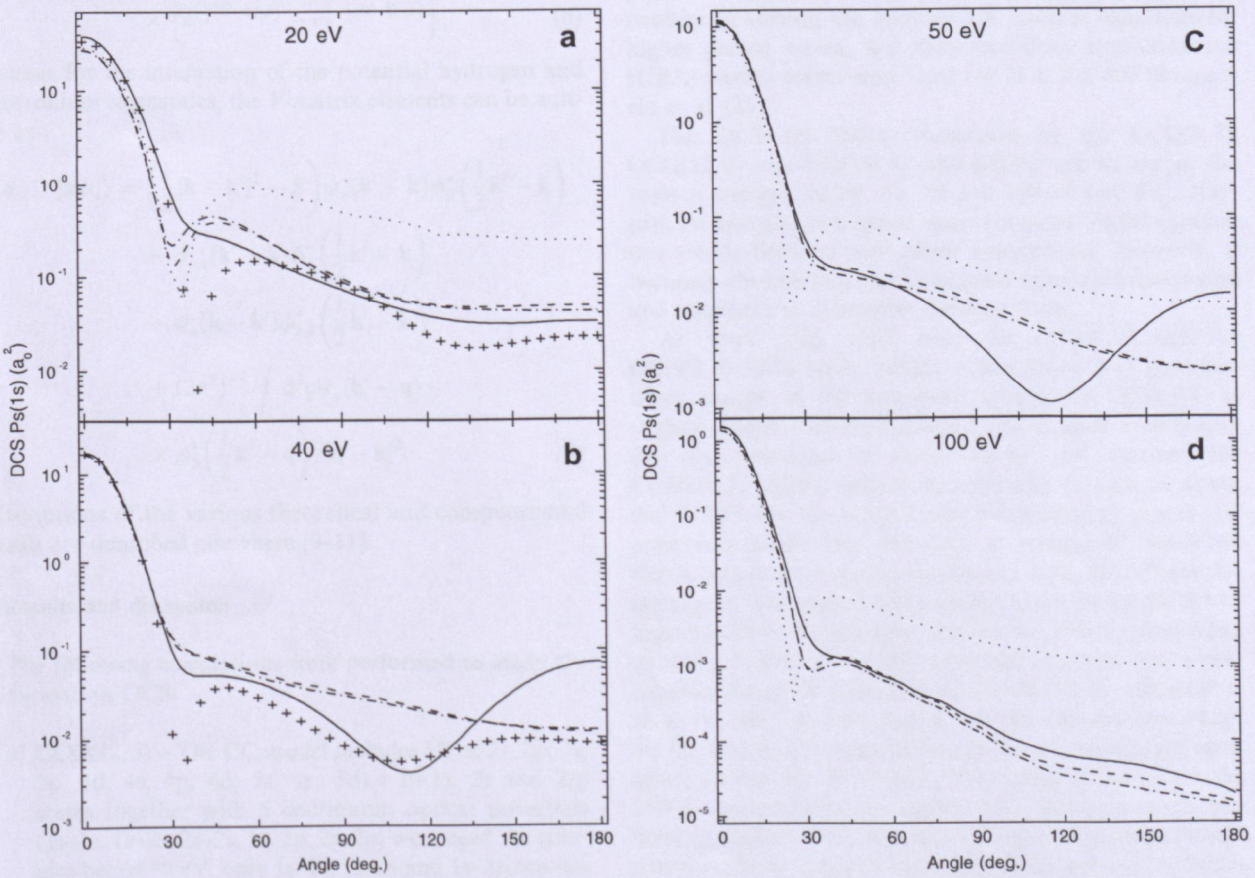

Fig. 1. (a) and (b): The DCS Ps(1s) formation for e^+–H scattering at 20 and 40 eV. Theoretical data: (—) CCO(12,3), (----) CCO(9,6), (-.-.-) CCO(9,3), (+ + +) Schwinger [16] and (...) DWA [12]. (c) and (d): The DCS Ps(1s) formation for e^+–H scattering at 50 and 100 eV. Theoretical data: (—) CCO(12,3), (----) CCO(9,6), (-.-.-) CCO(9,3) and (...) DWA [12].

$$\langle \mathbf{k}'\phi_{\beta'}|T|\mathbf{k}\psi_{\alpha}\rangle = \langle \mathbf{k}'\phi_{\beta'}|V|\mathbf{k}\psi_{\alpha}\rangle + \sum_{\alpha''}\int \mathrm{d}^3k'' \frac{\langle \mathbf{k}'\phi_{\beta'}|V|\mathbf{k}''\phi_{\alpha'}\rangle\langle \mathbf{k}''\psi_{\alpha''}|T|\mathbf{k}\psi_{\alpha}\rangle}{\left(E^{(+)} - \epsilon_{\alpha''} - \frac{1}{2}k''^2\right)} + \sum_{\beta''}\int \mathrm{d}^3k'' \frac{\langle \mathbf{k}'\phi_{\beta'}|V|\mathbf{k}''\phi_{\beta''}\rangle\langle \mathbf{k}''\phi_{\beta''}|T|\mathbf{k}\psi_{\alpha}\rangle}{\left(E^{(+)} - \epsilon_{\beta''} - \frac{1}{4}k''^2\right)}, \tag{4}$$

where $V^{(Q)}$ is the optical potential. The $\langle \mathbf{k}'\psi_{\alpha'}|T|\mathbf{k}\psi_{\alpha}\rangle$ and $\langle \mathbf{k}'\phi_{\beta'}|T|\mathbf{k}\psi_{\alpha}\rangle$ are the T-matrix elements for the transition from one channel state to the other.

The V-matrix elements in Eqs. (3) and (4) are defined as:

The potential for the interaction from the initial hydrogen eigen state to the final hydrogen eigen state is

$$\langle \mathbf{k}'\psi_{\alpha'}|V|\mathbf{k}\psi_{\alpha}\rangle = \frac{1}{(2\pi)^3}\int \mathrm{d}^3r_1 \int \mathrm{d}^3r_2 \psi^*_{\alpha'}(\mathbf{r}_1)\mathrm{e}^{-\mathrm{i}\mathbf{k}'\cdot\mathbf{r}_2} \times \left(\frac{1}{r_2} - \frac{1}{r_{12}}\right)\psi_{\alpha}(\mathbf{r}_1)\mathrm{e}^{\mathrm{i}\mathbf{k}\cdot\mathbf{r}_2}. \tag{5}$$

The direct interaction for Ps–proton scattering is

$$\langle \mathbf{k}'\phi_{\beta'}|V|\mathbf{k}\phi_{\beta}\rangle = \frac{1}{2\pi^2|\mathbf{k}-\mathbf{k}'|^2}\int \mathrm{d}^3\rho\,\phi_{\beta'}(\rho)\phi_{\beta}(\rho) \times \left\{\mathrm{e}^{\left(\frac{1}{2}\mathrm{i}(\mathbf{k}'-\mathbf{k})\cdot\rho\right)} - \mathrm{e}^{\left(-\frac{1}{2}\mathrm{i}(\mathbf{k}'-\mathbf{k})\cdot\rho\right)}\right\}, \tag{6}$$

whereas for the interaction of the potential hydrogen and positronium eigenstates, the V-matrix elements can be written as

$$\langle \mathbf{k}'\phi_{\beta'}|V|\mathbf{k}\psi_{\alpha}\rangle = \left(\frac{1}{2}|\mathbf{k}-\mathbf{k}'|^2 - E\right)\psi_{\alpha}(\mathbf{k}'-\mathbf{k})\phi^*_{\beta}\left(\frac{1}{2}\mathbf{k}'-\mathbf{k}\right) - \psi_{r,\alpha}(\mathbf{k}'-\mathbf{k})\phi^*_{\beta}\left(\frac{1}{2}\mathbf{k}'-\mathbf{k}\right) - \psi_{\alpha}(\mathbf{k}-\mathbf{k}')\phi^*_{r,\beta}\left(\frac{1}{2}\mathbf{k}'-\mathbf{k}\right) + (2\pi^2)^{-1}\int \mathrm{d}^3q\,\psi_{\alpha}(\mathbf{k}'-\mathbf{q}) \times \phi^*_{\beta}\left(\frac{1}{2}\mathbf{k}'-\mathbf{q}\right)/|\mathbf{q}-\mathbf{k}|^2. \tag{7}$$

Descriptions of the various theoretical and computational details are described elsewhere [9–11].

3. Results and discussion

The following calculations were performed to study the Ps formation DCS:

(a) CCO(12,3) – The CC model includes H(1s, 2s, 2p, 3s, 3p, 3d, 4s, 4p, 4d, 5s, 5p, 5d) + Ps(1s, 2s and 2p) states together with 5 continuum optical potentials (1s–1s, 1s–2s, 2s–2s, 1s–2p, 2s–2p) were used. At energies below 30 eV, only 1s–1s, 1s–2s and 1s–2p continuum channels were used.

(b) CCO(9,3) – This is similar to (a) except that only 9 H(1s, 2s, 2p, 3s, 3p, 3d, 4s, 4p, 4d) states + Ps(1s, 2s and 2p) and 5 optical potentials (1s–1s, 1s–2s, 2s–2s, 1s–2p, 2s–2p) were used. At energies below 30 eV, only 1s–1s, 1s–2s and 1s–2p continuum channels were used.

(c) CCO(9,6) – This is similar to (b) except that there are additional Ps(3s, 3p and 3d) states.

The calculations were done at the energy regime of 20–100 eV using the procedure of Ratnavelu et al. [15] that utilizes a five-panel composite mesh to generate sufficient quadrature points near the e^+–H and Ps–p on-shell momenta. A set of converged results were obtained with 68–84 quadrature points for $E < 100$ eV. However, at 100 eV, at least 92 quadrature points were needed. In the calculations, the Ps matrix elements were included until the angular momentum $J \leqslant 22$. The coupled LS integral equations were then solved for $0 \leqslant J \leqslant J_{MAX}$ with $J_{MAX} = 70$ at 100 eV. The continuum optical potentials were only allowed for $0 \leqslant J \leqslant J_{OPT}$. At 100 eV, J_{OPT} is 25. Although $J_{MAX} = 70$ seems sufficient for the calculations, however, we noticed small oscillations at large angles DCS for the Ps(1s) and Ps(2s) formation at 100 eV. These oscillations only disappeared with the inclusion of large partial waves in the calculations. Due to the numerical difficulties in solving the coupled LS integral equations for higher partial waves, the unitarised Born approximation (UBA) partial waves were used for $71 \leqslant J \leqslant 400$ (Ratnavelu et al. [15]).

The DCS for Ps(1s) formation by the CCO(9,3), CCO(12,3) and CCO(9,6) calculations are shown at the various energies of 20, 40, 50 and 100 eV (see Fig. 1(a)–(d)). At first glance it seems there are some similar qualitative trends between both these calculations. However, it becomes obvious that there are some significant qualitative and quantitative differences between them.

At 20 eV (Fig. 1(a)), both the CCO(9,3) and the CCO(9,6) DCS seem similar qualitatively and quantitatively except at the minimum where the CCO(9,6) is slightly deeper than the CCO(9,3). Both these models predict the minimum at about 30–35°. In contrast, the CCO(12,3) shows only a shoulder-like feature at about the 40–45°. On the other hand, the Schwinger model [16] predicts a deeper first minimum at around 40° while the DWA [12] shows a shallow minimum in the 30–35° scattering region. The second wide minimum shown by the Schwinger model is not demonstrated in the DWA calculations as well as the CCO models. However, it seems that a perceptible trough is materializing for the CCO calculations at about the 130–140° region. All the calculations except for the CCO(12,3), also show a prominent secondary maximum in the 40–50° region. It is quite evident that the DWA overestimates the middle and backward cross sections at angles >50° compared to other theoretical works which leads to a larger integrated cross section for Ps(1s) formation at $3.67\pi a_0^2$ whereas the CCO(12,3), CCO(9,3) and CCO(9,6) cross sections are $2.94\pi a_0^2$, $2.03\pi a_0^2$ and $2.04\pi a_0^2$, respectively. Thus, the present CCO Ps(1s) inte-

grated cross sections are within 20–25% closer to the larger L^2 (CC($\overline{28}$, 3) and CC($\overline{30}$, 3)) cross sections of $2.564\pi a_0^2$ at 20.41 eV and $2.55\pi a_0^2$ at 20.55 eV, respectively. The effect of increasing the three Ps states CCO(9,3) to six Ps states in CCO(9,6) barely affects the Ps(1s) formation at 20 eV.

At 40 eV (Fig. 1(b)), there is some minor differences between the CCO(9,3) and CCO(9,6) suggesting the effects of the inclusion of Ps($n = 3$) states are quite small but qualitatively they seem very similar. Similarity between the CCO(12,3) and the Schwinger [16] model is also seen except for the first minimum. The CCO(12,3) minima is quite shallow in comparison with that of the Schwinger model. The second wide minimum becomes clearly evident for the CCO(12,3) model. However this is not demonstrated by the CCO(9,3) or the CCO(9,6). There was no DWA [12] calculation reported at 40 eV. The integrated cross sections for Ps(1s) at 40 eV also reveal interesting findings. The present CCO(12,3), CCO(9,6) and CCO(9,3) cross sections of $0.846\pi a_0^2$, $0.905\pi a_0^2$ and $0.838\pi a_0^2$, respectively are about 25–40% higher than the CC($\overline{30}$, 3)($0.680\pi a_0^2$) and the CC($\overline{28}$, 3)($0.616\pi a_0^2$) integrated Ps(1s) cross sections. Furthermore at 40 and 50 eV (Fig. 1(c)), significant differences are noticeable between the DWA [12], Schwinger model [16], CCO(9,3), CCO(9,6) and the CCO(12,3) models especially at backward angles.

At 100 eV (Fig. 1(d)), the CCO(9,3), CCO(9,6) and CCO(12,3) again begin to demonstrate the distinctive minimum at the forward scattering angles. The present backward DCS sometimes show strong differences with the DWA [12]. The present integrated cross sections (CCO(12,3), CCO(9,6) and CCO(9,3) cross sections of $0.05\pi a_0^2$, $0.046\pi a_0^2$ and $0.041\pi a_0^2$, respectively) also differ significantly with the L^2 (CC($\overline{30}$, 3) and CC($\overline{28}$, 3)) cross sections of $0.026\pi a_0^2$ and $0.035\pi a_0^2$. It must be noted that the DWA cross section is $0.049\pi a_0^2$ which is closer to the present calculations. Thus, even at 100 eV, the DCS for the Ps(1s) is still unclear based on the comparison of these various integrated cross sections.

The DCS for Ps(2s) formation at 20, 40, 50 and 100 eV are depicted in Fig. 2(a)–(d), respectively. At 20 eV (see Fig. 2(a)), the present CCO(9,3) and CCO(9,6) calculations and the DWA [12] agreement are only limited to

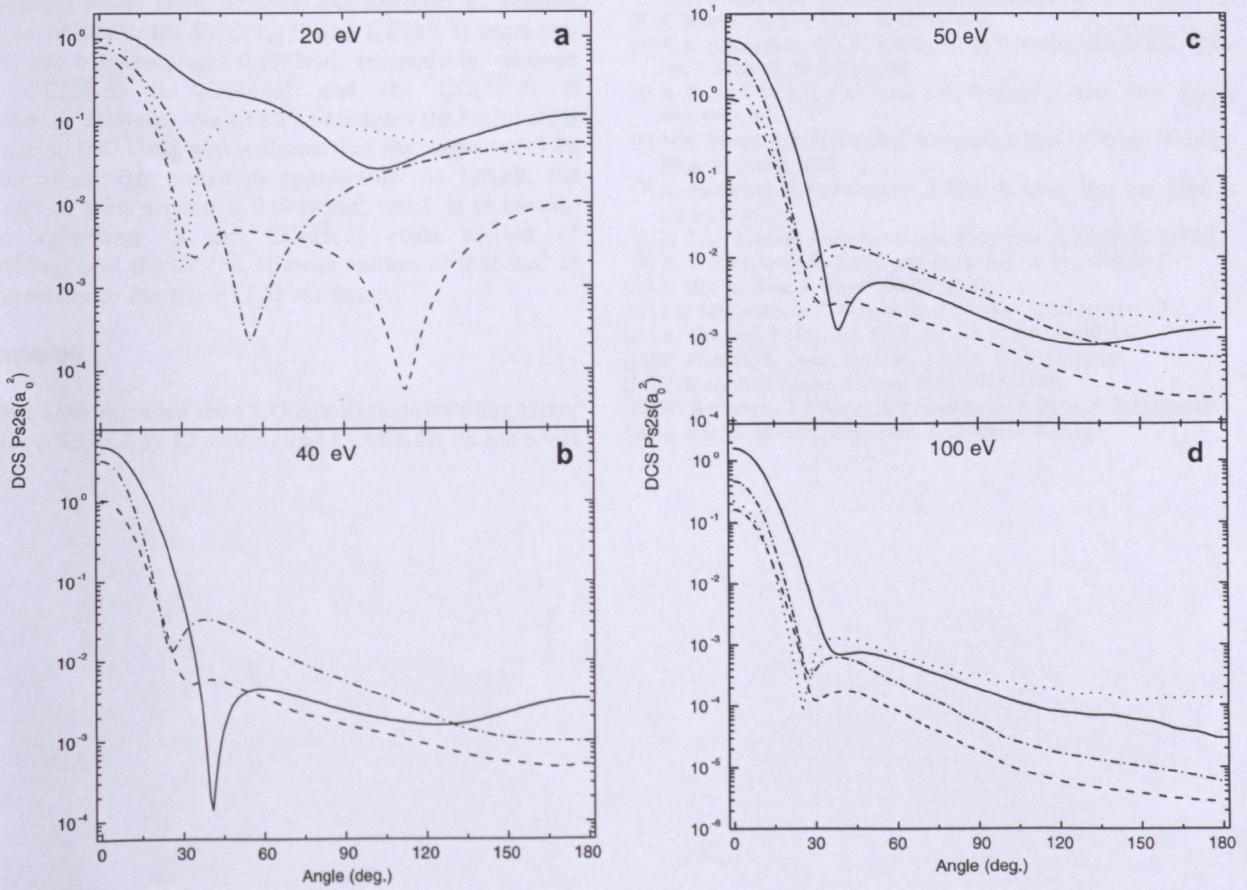

Fig. 2. (a) and (b): The DCS Ps(2s) formation for e^+–H scattering at 20 and 40 eV. Theoretical data: (—) CCO(12,3), (----) CCO(9,6), (-.-.-) CCO(9,3) and (...) DWA [12]. (c) and (d): The DCS Ps(2s) formation for e^+–H scattering at 50 and 100 eV. Theoretical data: (—) CCO(12,3), (----) CCO(9,6), (-.-.-) CCO(9,3) and (...) DWA [12].

the existence of the deep minimum at forward scattering angles. The qualitative and quantitative differences are quite glaring! In contrast to the DWA and CCO(9,3), the CCO(12,3) shows only a slight shoulder at lower angles with shallower trough at intermediate angles. As the incident energy increases, the CCO models seem to be in better accord qualitatively with the DWA except for the backward scattering angles. The differences between the CCO models at 40 eV (see Fig. 2(b)) is quite perturbing. Convergence studies suggest that the CCO(12,3) tends to increase the forward peak and the first minimum is much deeper than the others.

At higher incident energies of 50 (see Fig. 2(c)) and 100 eV (see Fig. 2(d)), the CCO models are more consistent with each other and with the DWA [12] model. The effect of including the Ps($n = 3$) states in the CCO(9,6) calculation reduces the forward peak appreciably. All calculations show similar behaviour with the DWA cross section which is larger at angles 60–170°.

However, in studying the integrated cross sections for Ps(2s) formation we can get a better insight on the quality of the present work. It is quite certain that the present CCO(12,3) and CCO(9,3) models are overestimating the integrated Ps(2s) cross sections. For example at incident energy of 50 eV, the CCO(12,3) and CCO(9,3) cross sections are $0.2588\pi a_0^2$ and $0.1133\pi a_0^2$, respectively, whereas the CC($\overline{28}$,3) is $0.0644\pi a_0^2$ and the CC($\overline{30}$,3) is $0.0569\pi a_0^2$. However, the CCO(9,6) reduces the Ps(2s) cross section to $0.0394\pi a_0^2$ which shows that the larger $n = 3$ Ps states affects this transition appreciably. At 100 eV, the CCO(9,6) cross section is $0.00496\pi a_0^2$ which is in reasonable agreement to the CC($\overline{28}$,3) cross section of $0.0063\pi a_0^2$ and the CC($\overline{30}$,3) cross section of $0.053\pi a_0^2$ in comparison to the other CCO models.

Conclusion

We have extended the CCO calculations by using larger states (CCO(12,3), CCO(9,3) and CCO(9,6)) on the e^+–H scattering at energies ranging from 20 to 100 eV. The continuum optical potentials were used in all calculations. In the present work, the Ps(1s) DCS shows comparable quantitative agreement with other theories at intermediate energies >20 eV to some extent except at backward angles. However, the present CCO calculations of Ps(2s) DCS is quite lacking in comparison with the DWA [12] for $E > 20$ eV. Other theoretical reports should endeavour to report the DCS for positron–hydrogen scattering system so as to provide a more discriminatory test for theories.

Acknowledgements

K.R. acknowledges the funding by the Academy of Science Malaysia (SAGA Grant 66-02-03-0077). M.Z.M.K. and K.R. also acknowledge support from University of Malaya.

References

[1] M. Charlton, J.W. Humberston, Positron Physics, Cambridge University Press, 2000.
[2] G. Laricchia, M. Charlton, in: P.G. Coleman (Ed.), Positron Beams and its Applications, World Scientific, 2000, p. 41.
[3] J. Mitroy, Aust. J. Phys. 49 (1996) 919.
[4] A.A. Kernoghan, D.J.R. Robinson, M.T. McAlinden, H.R.J. Walters, J. Phys. B. 29 (1996) 2089.
[5] B. Zhou, C.D. Lin, J.Z. Tang, C.K. Kwan, T.S. Stein, Phys. Rev. A 55 (1997) 361.
[6] N.R. Hewitt, C.J. Noble, B.H. Bransden, J. Phys. B: Atom. Mol. Opt. Phys. 23 (1990) 1485.
[7] K. Ratnavelu, K.K. Rajagopal, J. Phys. B: Atom. Mol. Opt. Phys. 32 (1999) L381.
[8] M.Z.M. Kamali, Kuru Ratnavelu, Phys. Rev. A 65 (2002) 014702.
[9] K.K. Rajagopal, K. Ratnavelu, Phys. Rev. A 62 (2000) 022717.
[10] J. Mitroy, Aust. J. Phys. 46 (1993) 751.
[11] I.E. McCarthy, A.T. Stelbovics, Phys. Rev. A 28 (1983) 2693.
[12] A. Ghoshal, P. Mandal, Phys. Rev. A 72 (2005) 032714.
[13] P. Mandal, S. Guha, N.C. Sil, J. Phys. B 12 (1979) 2913.
[14] P. Mandal, S. Guha, J. Phys. B 12 (1979) 1603.
[15] K. Ratnavelu, J. Mitroy, A.T. Stelbovics, J. Phys. B 29 (1996) 2775.
[16] S. Kar, P. Mandal, Phys. Rev. A 62 (2000) 052514.